# Brief review of metal nanoclusters in block copolymer films†

**J. F. Ciebien,‡ R.T. Clay,§ B.H. Sohn¶ and R. E. Cohen***

*Department of Chemical Engineering, Massachusetts Institute of Technology, Cambridge, MA 02139, USA*

We provide a brief non-comprehensive survey of some recent work on the *in situ* production of metal nanoclusters in polymer films. The synthesis schemes rely on the well-known spontaneous microphase separation of block copolymers to restrict metal species within nanoscale regions in the bulk morphology. In one variation of the scheme, organometallic monomers are used to form one of the block sequences of the block copolymer. A second approach relies on metal-sequestering moieties in one of the blocks which assemble to produce 'nanoreactors' capable of being loaded with metal species for later reduction to zerovalent clusters. Morphological evidence is provided to assess the success of these schemes. A few properties of the metal-containing nanocomposite films are discussed here. These include electrical properties and catalytic activity in hydrogenation reactions.

There has been growing interest during recent years in materials with characteristic length scales on the order of nanometers. Nanoclusters are the subject of research and product development because they may possess interesting and useful catalytic,[1–5] magnetic,[6–8] optical,[9–13] nonlinear optical,[14,15] semiconductor[16] or other properties. Nanoclusters are small particles of metal, metal oxides or semiconductor materials; the size range of interest is usually 10–500 Å in diameter. These materials often display properties intermediate between the bulk and the atom, arising from quantum size effects[16–18] or the large surface area-to-volume ratio[19] of very small particles.

The study of nanocomposite materials for applications such as catalysts, UV-absorbing coatings and capacitors often requires that the clusters be uniformly sized and homogeneously distributed throughout a dielectric support. A narrow cluster size distribution is helpful to study size-dependent properties and a dielectric support prevents electronic interactions between the clusters and other conductive materials. Further, the clusters must be stabilized against aggregation and growth to maintain the performance of the composite material within engineering specifications.

Polymers are often used as a stabilizing matrix for nanoclusters. Most polymers are easily processable and a transparent, permeable, or conductive material can be chosen, as required for specific applications. Polymer–metal cluster nanocomposites have been synthesized by condensation of metal vapors into liquid monomer, which is later polymerized,[20,21] by reduction of metal complexes in solution where the solvent also acts as a polymerizable ligand,[22] and by simultaneous metal evaporation and plasma polymerization.[23] Supercritical $CO_2$ solutions have also been used to load bulk polymer films with metal salts and to reduce these salts to metal nanoclusters by chemical post-treatment.[24]

Recently, methods of synthesizing nanoclusters in microphase-separated diblock copolymers[25–37] have been reported that provide greater control over cluster formation. Möller[25] has prepared metal sulfide clusters within microphase-separated diblock copolymers of polystyrene and poly-2-vinylpyridine. Sulfides of Cu, Cd, Co, Ni, Zn and Ag were prepared by solvent evaporation from solutions containing the diblock copolymer and a metal salt, followed by treatment with gaseous $H_2S$. The metal salts formed complexes with the pendant pyridine rings, concentrating the metal ions in the poly-2-vinylpyridine domains and leading to the well-controlled formation of sulfide nanoclusters within the films.

Spatz *et al.*[27] have used diblock copolymer micelles to form polymer films containing well-ordered arrays of gold nanoclusters with a narrow size distribution. Polystyrene-*block*-poly(ethylene oxide) was dissolved in toluene, forming a diblock copolymer micellar solution. When $LiAuCl_4$ is added to the solution, $Li^+$ ions form complexes with PEO repeat units, thus binding the $[AuCl_4]^-$ ions within the core of the micelles. Polymer thin films were formed by placing a small drop of the micellar solution on a TEM grid. Transmission electron microscopy revealed that the micelles had organized into a near-perfect hexagonal array. Annealing the sample resulted in formation of a single gold nanocluster within each diblock copolymer micelle. Kinetic control over the polymer film morphology proved an effective means of arranging the nanoparticles in an ordered array. Further, the size of the nanoclusters could be controlled by varying the volume fraction of each block or the $LiAlCl_4$ : EO ratio.

Past work in our group has focused on the synthesis of metal,[28–30] metal oxide[31,32] and semiconductor[33–40] nanoclusters within the microdomains of block copolymers prepared by ring-opening metathesis polymerization (ROMP). In this review we focus on recent observations and applications for the case of the zero-valent metal clusters. Our technique capitalizes on the formation of self-assembled microdomains within diblock copolymers. Organometallic repeat units comprising one of the blocks are reduced by chemical treatment, leading to formation of metal nanoclusters predominantly within the original organometallic domains.[28–30] The polymer morphology (lamellar, cylindrical or spherical) and domain size are determined by the volume fraction of each block and the total molecular weight of the block copolymer. Optimum control over cluster formation is achieved by using a film with

† Non-SI unit employed: 1 psi = 0.069 bar = $6.9 \times 10^3$ Pa.

‡ Present address: Bayer Corporation, Polymers Division, 100 Bayer Road, Pittsburgh, PA 15205-9741, USA.

§ Present address: Mobil Technology Company, 600 Billingsport Road, Paulsboro, NJ 08066-0480, USA.

¶ Present address: Department of Chemical Engineering, University of Winconsin at Madison, 1415 Johnson Drive, Madison, WI 53706, USA.

a spherical morphology; films containing a single cluster within each spherical domain have been prepared.[28]

A more general method for the synthesis of several transition metal nanoclusters (Ag, Au, Cu, Ni, Pb, Pd and Pt) has also been developed.[41] Metal ions or complexes are coordinated to carboxylic acid groups within the hydrophilic blocks of a diblock copolymer by immersion of the polymer in an aqueous metal salt solution. The metal ions or complexes are subsequently reduced by exposure to hydrogen at elevated temperatures or by immersion in an aqueous sodium borohydride solution. For several transition metals, this approach leads to uniformly sized nanoclusters homogeneously dispersed within the water-soluble domains.

## Organometallic Block Copolymers

The interfaces between dissimilar domains and the free interfaces of thin films both play an important role in nucleation and growth of clusters formed *in situ* within microphase-separated diblock copolymers. Silver clusters have been formed under several different conditions using bulk films (static-cast) and thin films (microtomed or spin-coated).[42]

TEM (Fig. 1) and small-angle X-ray scattering (SAXS) analysis[43] of an $[Ag]_{60}[MTD]_{300}$ bulk block copolymer film revealed a lamellar morphology with a domain size of about 21 nm. Ag refers to the repeat unit of the silver-containing block of the copolymer, $Ag_2(Hfacac)_2NORPHOS$, where NORPHOS = racemic 2-*exo*-3-*endo*-bis(diphenylphosphino) bicyclo[2.2.1]heptane and MTD = methyltetradodecene. The bulk film was thermally treated to produce silver nanoclusters. The transmission electron micrograph given in Fig. 2 shows that silver nanoclusters formed predominantly within the original silver-containing microdomains with no disruption in the original lamellar morphology. Wide-angle X-ray scattering (WAXS) analysis confirmed that the clusters are zero-valent silver in the cubic form.[43] When a similar cluster synthesis was carried out in bulk films of metal-containing homopolymers, the cluster formation was not well-controlled; large clusters with a broad size distribution were obtained and the clusters were not dispersed homogeneously throughout the metal-containing homopolymer films.[30] These results indicate that the interfaces between blocks in a microphase-separated diblock copolymer can act as favored cluster nucleation sites. Because these interfaces are regularly spaced, the clusters form uniformly throughout the block copolymer films. Moreover, confinement within the lamellae can control the growth of clusters by reducing the local supply of silver.

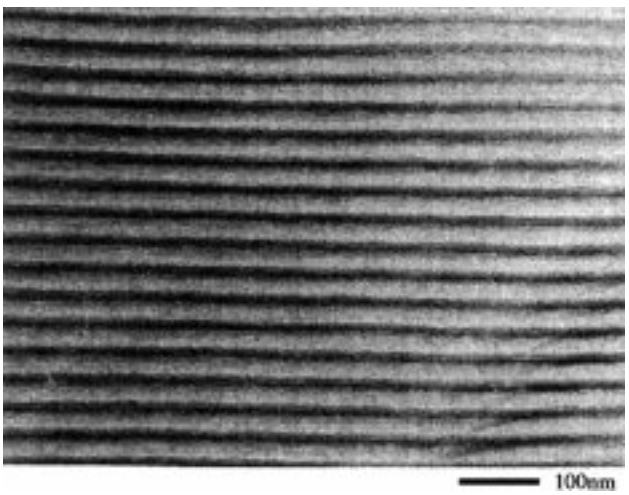


**Fig. 1** Transmission electron micrograph of $[Ag]_{60}[MTD]_{300}$. (Reproduced from ref. 43(*b*) with permission of the author)

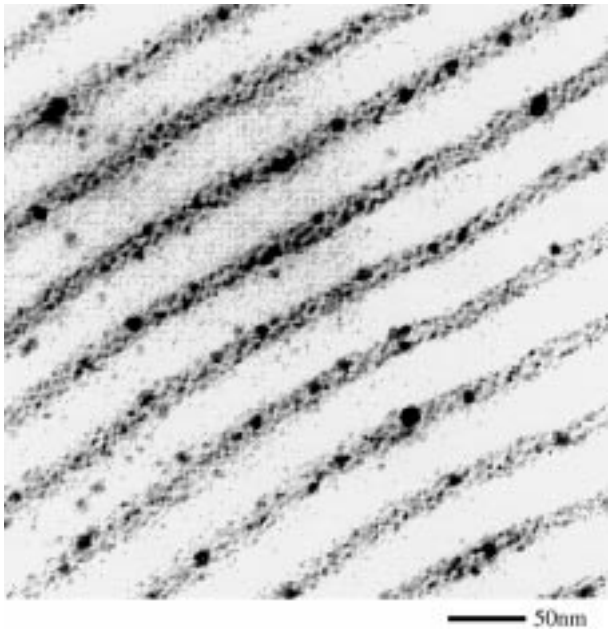


**Fig. 2** Transmission electron micrograph of $[Ag]_{60}[MTD]_{300}$ after cluster formation; reduced as a bulk film (*ca.* 100 μm thick). (Reproduced from ref. 43(*b*) with permission of the author)

If the thickness of a metal-containing homopolymer film is reduced close to the dimensions of lamellae in block copolymers, the 'free interfaces', that is the surfaces of the thin films, can play a role similar to that of the interdomain interfaces in block copolymers. Thus, small uniformly sized clusters are expected to form within metal-containing homopolymers if the film thickness is small enough. An $[Ag]_{80}$ homopolymer film thin enough (*ca.* 100 nm) to obtain a TEM micrograph without microtoming was prepared by spin-coating. Before cluster formation, there was no visible contrast in the TEM micrograph. After cluster formation, relatively small (*ca.* 5 nm in diameter), irregularly shaped clusters were obtained throughout the film (Fig. 3). The film surfaces evidently did play a similar role in cluster formation as the interfaces between blocks in block copolymers, so that similarly small clusters were produced both in the spin-coated film of homopolymer $[Ag]_{80}$ and in the bulk film of diblock $[Ag]_{60}[MTD]_{300}$. The spin-coated film of $[Ag]_{80}$ is essentially analogous to a single lamella of [Ag] blocks in $[Ag]_{60}[MTD]_{300}$. Both can be considered as regions of con-

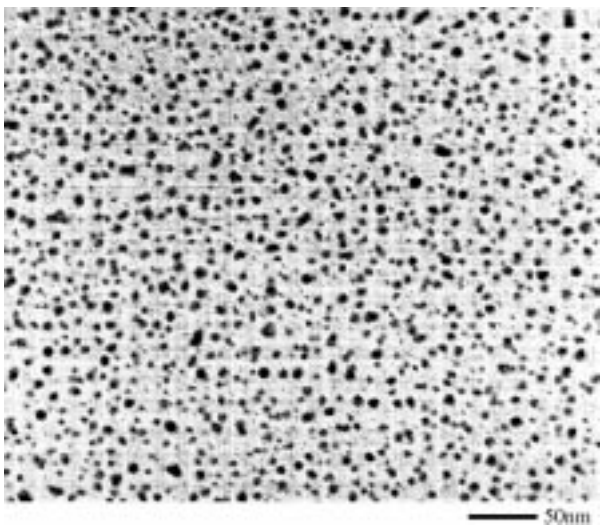


**Fig. 3** Transmission electron micrograph of the spin-coated film of $[Ag]_{80}$ after cluster formation (*ca.* 100 nm thick). (Reproduced from ref. 43(*b*) with permission of the author)

fined cluster growth in which there is only a two-dimensional supply of silver and a readily accessible interface for heterogeneous cluster nucleation.

Taking thin sections of a bulk film of $[Ag]_{60}[MTD]_{300}$ before cluster formation is essentially the same as adding new 'free interfaces' to the existing interfaces between blocks; the [Ag] block can then be thought of as a one-dimensional rectangular channel of nanoscopic dimensions. Reduction of the silver in these channels (*ca.* 50 nm × 25 nm) resulted in a narrower cluster size distribution (*ca.* 5 nm in diameter) than that observed in Fig. 2 and 3. This was apparently the result of more nucleation sites and fewer available silver atoms per nucleation site.

## Electrical Properties

Nanocomposite materials with conducting nanoparticles embedded in a nonconducting polymer matrix may have interesting electrical properties. In particular, microphase-separated diblock copolymer films displaying a well-ordered lamellar morphology may display highly anisotropic properties if the conducting clusters are confined within alternating lamellae. A bulk film of $[Ag]_{60}[MTD]_{300}$ was prepared by static-casting. TEM analysis showed a well-ordered lamellar morphology (Fig. 1) and SAXS studies indicated that most, but not all, lamellar planes were oriented parallel to the plane of the film. The $[Ag]_{60}[MTD]_{300}$ film was thermally treated to form clusters and the TEM micrograph after reduction showed that silver nanoclusters formed predominantly within the original silver-containing microdomains.

It is interesting to compare dielectric properties parallel and perpendicular to the film plane. In practice, however, it is not easy to measure dielectric properties parallel to the film plane because the film is only about 100 μm thick. However, if we knew the dielectric constant of each lamellar region, we could calculate the dielectric constant parallel to the film plane ($\varepsilon'_{\|}$) and confirm the measured value of the dielectric constant perpendicular to the film plane ($\varepsilon'_{\perp}$). $\varepsilon'_{\perp}$ can be modeled as a series combination of the dielectric constant of the [Ag] block ($\varepsilon'_{Ag}$) and the dielectric constant of the [MTD] block ($\varepsilon'_{MTD}$) (Fig. 4). Furthermore, $\varepsilon'_{\|}$ can be modeled as a parallel combination of $\varepsilon'_{Ag}$ and $\varepsilon'_{MTD}$. From series and parallel combinations of blocks, we can write

$$1/\varepsilon'_{\perp} = (t_{Ag}/t)/\varepsilon'_{Ag} + (t_{MTD}/t)/\varepsilon'_{MTD} \quad (1)$$

$$\varepsilon'_{\|} = (t_{Ag}/t)\varepsilon'_{Ag} + (t_{MTD}/t)\varepsilon'_{MTD} \quad (2)$$

where $t$ is the total film thickness, $t_{Ag}$ is the thickness of [Ag] domains and $t_{MTD}$ is the thickness of [MTD] domains (*i.e.*, $t = t_{Ag} + t_{MTD}$). From the TEM micrographs (Fig. 2), we can find $t_{Ag}/t = 0.455$ and $t_{MTD}/t = 0.545$.

The array of experimentally derived[43] values [$\varepsilon'_{Ag}$ (4.80), $\varepsilon'_{MTD}$ (2.88), $t_{Ag}/t$ (0.455), and $t_{MTD}/t$ (0.545)] can be inserted into eqn. (1) and (2). From eqn. (1), the calculated value of $\varepsilon'_{\perp}$ is 3.52, essentially identical with the measured value of $\varepsilon'_{\perp}$ at $10^4$ Hz. From eqn. (2), $\varepsilon'_{\|}$ is 3.76. Thus the dielectric constants

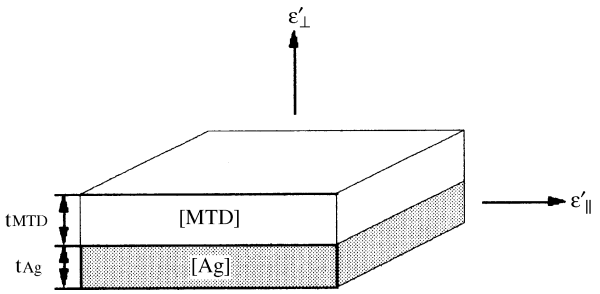


**Fig. 4** Schematic representation of the oriented lamellae of $[Ag]_{60}[MTD]_{300}$

for the static-cast film of $[Ag]_{60}[MTD]_{300}$ showed only a slight anisotropy ($\varepsilon'_{\perp} = 3.52$ *vs.* $\varepsilon'_{\|} = 3.76$). This result suggests that the silver clusters in the alternating domains are well below the percolation threshold. TEM photomicrographs offer a through-going view of several layers of clusters, thereby exaggerating the apparent proximity of the clusters.

Electrical conductivity measurements of a static-cast film of $[Ag]_{60}[MTD]_{300}$ were also performed.[44] $s_{\perp}$ was below the detection limit ($10^{-13}$ S cm$^{-1}$) in DC mode; the value was instead estimated at $2.2 \times 10^{-15}$ S cm$^{-1}$ by extrapolation of AC measurements to $10^{-3}$ Hz. The values of $s_{\|}$ were around $10^{-9}$ S cm$^{-1}$. The order of magnitude of $s_{\|}$ is reasonable when the silver content (30 wt% within microdomains) is considered.[44,45] The conductivity of the $[Ag]_{60}[MTD]_{300}$ film is highly anisotropic.

## Catalysis

Palladium nanoclusters[30] have been synthesized by reduction of microphase-separated diblock copolymer films of $[MTD]_{113}[Pd]_{50}$. The catalytic activity of the resulting nanocomposite materials for gas phase, heterogeneous hydrogenation reactions has been measured.[46,47] Two catalyst films, A and B, were prepared containing an equal weight fraction palladium but differing in cluster size. TEM analysis showed that the clusters in catalyst film A had an average diameter of 30 Å and appeared to form preferentially within the original organometallic domains. Catalyst film B contained clusters of *ca.* 14 Å diameter. The clusters were again examined by TEM after being used as ethylene hydrogenation catalysts. The average cluster diameter for catalyst A after ten ethylene hydrogenation runs was unchanged at 30 Å, whereas the average cluster diameter in B increased from 14 to 19 Å after eight experimental runs.

To study the catalyst activity as a function of cluster size, batch mode ethylene hydrogenation reactions were performed. The activity of each catalyst was calculated as the moles of ethylene consumed per mole palladium per second. The maximum activity for each run, as calculated from pairs of consecutive data points, is reported in Table 1, along with the mean and standard deviation for each catalyst.

The mean activity of catalyst A for ethylene hydrogenation was $0.0012 \pm 0.0004$ mol (mol Pd)$^{-1}$ s$^{-1}$, while that of catalyst B was $0.0021 \pm 0.0005$ mol (mol Pd)$^{-1}$ s$^{-1}$ (see Table 1). There was no trend towards loss of activity with repeated use of the catalysts, indicating that the active sites are not deactivated by, for example, carbonaceous deposits during the reaction. On average, catalyst B is 1.8 times more active than catalyst A. This difference in activity can be explained by differences in the total palladium surface area between the catalysts. Both catalysts contain the same weight fraction palladium; therefore, the ratio of the total palladium surface

**Table 1** Catalyst activity as a function of cluster size. Maximum activity for ethylene hydrogenation for catalysts A and B at 120 °C with $P_{H_2} = 30$ psi$_a$ and $P_{C_2H_4} = 15$ psi$_a$

| | Maximum activity/$10^{-3}$ mol (mol Pd)$^{-1}$ s$^{-1}$ | |
|---|---|---|
| Run | Catalyst A | Catalyst B |
| 1 | 2.0 | 2.0 |
| 2 | 0.69 | 1.3 |
| 3 | 0.98 | 1.6 |
| 4 | 1.3 | 2.5 |
| 5 | 1.3 | 2.7 |
| 6 | 1.1 | 2.5 |
| 7 | — | 1.6 |
| 8 | — | 2.3 |
| Mean | 1.2 | 2.1 |
| Std. dev. | 0.4 | 0.5 |

area in each catalyst can be estimated from the average cluster diameter, assuming that the clusters are spherical, and monodisperse, and that the organometallic repeat units have been reduced to the same extent. Using TEM cluster diameter measurements made before and after the ethylene hydrogenation experiments, catalyst **B** is expected to be 1.6–2.2 times more active than catalyst A, based solely on the difference in total palladium surface area. This result is in agreement with experimental observations.

Catalyst films **A** and **B** were also used for 1,3-butadiene hydrogenation reactions.[47] Repeated use of the catalysts for hydrogenation reactions had two main effects on the nanocomposite morphology. First, the palladium cluster diameter increased gradually; this increase was more dramatic for **B** with its smaller initial cluster size. The average cluster diameter of A was 35 Å after 27 hydrogenation runs and that of catalyst **B** was 32 Å after 32 experimental runs. There was no evidence that entire clusters migrated through the polymer matrix. Rather, it appeared that cluster growth was the result of migration of individual palladium atoms through the polymer matrix. The source of the palladium was either existing clusters or further reduction of previously unreacted pendent organometallic complexes. Secondly, exposure to $C_4$ gases also resulted in 15–60 μm voids opening up within the polymer matrix. Further study of ethylene hydrogenation[46,47] showed that the activity of the nanocomposite catalysts more than doubled after exposure to $C_4$ gases because the presence of the voids decreased the mean diffusion path length within the matrix, resulting in an increase in catalytic activity.

Table 2 summarizes the maximum activity and butene selectivity for catalyst A at 120 °C and with a hydrogen : butadiene ratio of 4 : 1, 1 : 1 or 1 : 2. The data clearly show that the selectivity for butenes over *n*-butane increases as the hydrogen partial pressure decreases. The product distribution data summarized in Table 3 show that the *trans*-2-butene and *cis*-2-butene selectivities change little with reactant partial pressure, but that the selectivity for 1-butene increases significantly with decreasing $P_{H_2}$. Therefore, the overall loss of butene selectivity with increasing hydrogen partial pressure can be attributed to an increase in the rate of hydrogenation of 1-butene to *n*-butane.

Reactions were also run at 120 °C and $P_{H_2} = P_{C_4H_6} = 15$ $psi_a$, on films that had received similar exposure to $C_4$ gases. The higher activity of catalyst **B** (Table 4) can again be explained by the greater total palladium surface area available for reaction. A comparison of the data obtained at room temperature and 120 °C indicates that raising the reaction temperature by *ca.* 100 °C increases catalyst activity by one order of magnitude.[47]

The average product distributions reported in Table 5 for catalyst A and **B** at room temperature and 120 °C show that the *trans*-2-butene and *cis*-2-butene selectivities vary little with reaction temperature or cluster size. In contrast, the selectivity for 1-butene increases significantly at the lower reaction temperature and catalyst **B** has better selectivity for 1-butene than catalyst A. The consistently high *trans : cis* ratio for 2-butene production is typical of palladium catalysts.[48]

**Table 2** Maximum activity and selectivity of catalyst A for 1,3-butadiene hydrogenation at 120 °C and different $P_{H_2} : P_{C_4H_6}$ ratios

| $P_{H_2} : P_{C_4H_6}$ | Maximum activity[a]/ $10^{-2}$ mol (mol Pd)$^{-1}$ s$^{-1}$ | Maximum selectivity |
|---|---|---|
| 4 : 1 | 5.5 (1) | 0.67 |
| | 2.2 (2) | 0.57 |
| | 9.3 (3) | 0.55 |
| | 8.6 (4) | 0.60 |
| | 12 (5) | 0.70 |
| Mean | 7.5 | 0.62 |
| Std. dev. | 3.4 | 0.06 |
| 1 : 1 | 9.7 (6) | 0.81 |
| | 13 (7) | 0.88 |
| | 8.7 (8) | 0.85 |
| Mean | 10 | 0.85 |
| Std. dev. | 2 | 0.03 |
| 1 : 2 | 2.9 (9) | 0.99 |
| | 2.6 (10) | 0.96 |
| | 2.4 (11) | 0.96 |
| | 2.5 (12) | 0.92 |
| Mean | 2.6 | 0.96 |
| Std. dev. | 0.2 | 0.02 |

[a] Experimental run numbers are given in parentheses.

**Table 3** Summary of reactant partial pressures and average product distributions (%) for catalyst A at 120 °C

| $P_{H_2}$/$psi_a$ | $P_{C_4H_6}$/$psi_a$ | 1-Butene | *trans*-2-Butene | *cis*-2-Butene | *n*-Butane |
|---|---|---|---|---|---|
| 40 | 10 | 20 | 30 | 11 | 39 |
| 15 | 15 | 27 | 39 | 18 | 16 |
| 10 | 20 | 45 | 35 | 16 | 4 |

## Nanoreactors

To avoid the synthesis of a new ROMP monomer each time a new type of metal cluster is desired in the polymer films, we have developed a general method for the synthesis of transition metal nanoclusters (specifically Ag, Au, Cu, Ni, Pb, Pd and Pt) using a single block copolymer.[41] In this strategy, metal ions or complexes are coordinated to carboxylic acid groups within hydrophilic polyNORCOOH domains of an $[MTD]_{400}[NORCOOH]_{50}$ diblock copolymer film. The ion sequestering is accomplished by immersing the film in an aqueous metal salt solution. Subsequent reduction of the metal ions by exposure to hydrogen at elevated temperatures, or immersion in an aqueous sodium borohydride solution, results in formation of nanoclusters with a narrow size distribution, uniformly distributed within the polyNORCOOH domains (see Fig. 5).

This 'universal' cluster synthesis technique uses the

**Table 4** Maximum activity and selectivity of catalysts A and **B** for 1,3-butadiene hydrogenation at 120 °C with $P_{H_2} = P_{C_4H_6} = 15$ $psi_a$

| | Maximum activity/$10^{-2}$ mol (mol Pd)$^{-1}$ s$^{-1}$ | | Maximum selectivity | |
|---|---|---|---|---|
| | Catalyst A | Catalyst **B** | Catalyst A | Catalyst **B** |
| | 9.7 | 27 | 0.81 | 0.90 |
| | 13 | 8.5 | 0.88 | 0.75 |
| | 8.7 | 8.9 | 0.85 | 0.88 |
| | | 31 | | 0.92 |
| Mean | 10 | 19 | 0.85 | 0.86 |
| Srd. dev. | 0.2 | 10 | 0.03 | 0.07 |

**Table 5** Average product distribution (%) of catalysts A and **B** at 20 °C or 120 °C with $P_{H_2} = P_{C_4H_6} = 15$ $psi_a$

| | 20 °C | | 120 °C | |
|---|---|---|---|---|
| Product | Catalyst A | Catalyst **B** | Catalyst A | Catalyst **B** |
| 1-Butene | 37 | 47 | 27 | 36 |
| *trans*-2-Butene | 30 | 34 | 39 | 35 |
| *cis*-2-Butene | 10 | 13 | 18 | 16 |
| *n*-Butane | 23 | 6 | 16 | 13 |

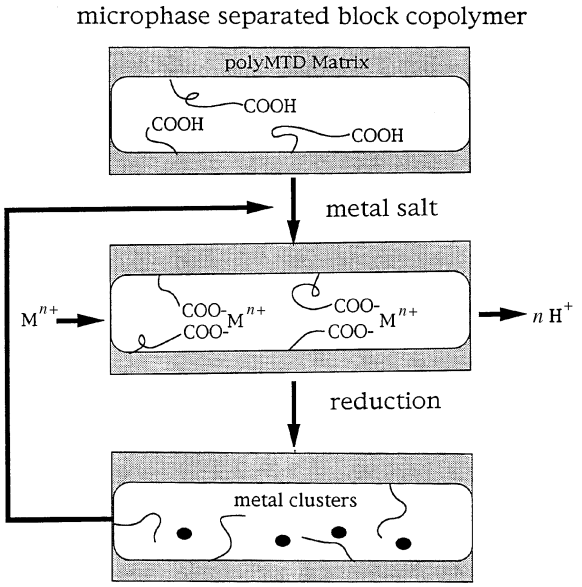


**Fig. 5** Block copolymer nanoreactor scheme for metal nanocluster synthesis

microphase-separated morphology of the diblock copolymer as a kinetic barrier to restrict cluster aggregation and migration out of the polyNORCOOH domains into the glassy polyMTD matrix ($T_g$ *ca.* 210 °C). The technique allows for the simple, *in situ* synthesis of several types of nanoclusters within a diblock copolymer matrix. Furthermore, the technique allows for the possibility of increasing cluster size and producing core-shell clusters through multiple loading and reduction cycles.

Bulk block copolymer samples and thin microtomed sections were loaded with metal ions or complexes by immersion in aqueous metal salt solutions and then reduced. The Ag-, Au-, Cu-, Pd- and Pt-containing films were also subjected to a second loading and reduction cycle. Prior to reduction, the faint outline of an interconnected cylindrical morphology was observed in the Ag-, Pd- and Pb-containing films. No such contrast between microdomains was visible in the Au-containing film. After the first loading and reduction cycle, uniformly sized silver (25–35 Å) and palladium (10–20 Å) clusters were observed and appeared to be restricted to the polyNORCOOH domains of each film. After a second loading and reduction cycle, the size of both the silver (40–90 Å) and palladium (20–30 Å) clusters increased, but they remained fairly uniformly sized and restricted to the polyNORCOOH domains.

The interconnected cylindrical morphology of the Au-containing film became visible after reduction of the film. Numerous gold clusters (10–15 Å) were observed in the polyNORCOOH domains and a few gold particles (200–500 Å) appeared to have grown beyond the polyNORCOOH domains. Fig. 6 shows transmission electron micrographs of the bulk Ag-containing film (*a*) after a single loading, (*b*) after a single loading and reduction sequence and (*c*) after the second loading and reduction sequence. The micrographs clearly demonstrate the ability to control and modify cluster size by use of the method outlined in Fig. 5.

All seven metal-loaded films were examined by WAXS before and after reduction. WAXS analysis of the Ag-loaded film showed that no fcc silver crystals formed prior to reduction. After one and two loading/reduction cycles, broad scattering peaks consistent with the [111], [200] and [220] planes of the fcc silver lattice[49] were observed. A mean crystal diameter of 40 Å was estimated from the Scherrer equation[50] for the twice loaded and reduced film. Comparison with TEM results indicates that many of the clusters in Fig. 6 are single crystals.

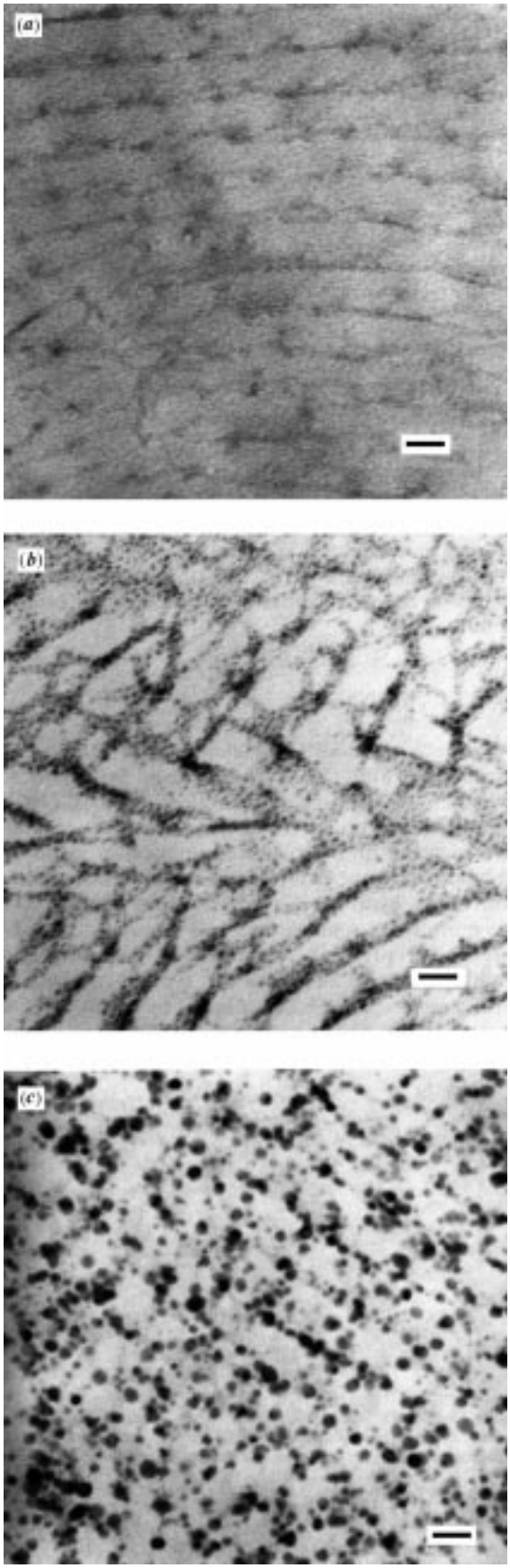


**Fig. 6** (*a*) Electron micrograph of bulk $Ag^+$ loaded film (bar = 300 Å). (*b*) Electron micrograph of bulk silver-containing film after first loading/reduction sequence (bar = 300 Å). (*c*) Electron micrograph of bulk silver-containing film after second loading/reduction sequence (bar = 300 Å)

WAXS analysis of the twice loaded and reduced Pd-containing film revealed a small peak consistent with scattering from the [111] plane of the fcc palladium lattice.[49] For the Au-loaded films, peaks consistent with the [111], [200] and [220] planes[49] of the gold fcc lattice were observed. An increase in the sharpness of the gold scattering peaks and a slight upturn in the WAXS data at low angles are indicative of the presence of large (several hundred Angstroms) gold clusters in the twice loaded and reduced films. Very few such clusters were observed by TEM, however, and it is possible that these large clusters occur preferentially near the surface of the bulk films where they would not be observed by TEM.

WAXS data from the once loaded and reduced Pb- and Ni-containing films exhibited only a single broad peak due to scattering from the amorphous polymer matrix. The Pt- and Cu-containing films exhibited only a single amorphous scattering peak after two loading and reduction cycles. Because contrast was observed by TEM in the Pb-loaded film, it is believed that the aqueous $NaBH_4$ was unable to penetrate the film in sufficient quantity to reduce lead or nickel ions. The absence of Pt clusters is attributed to slow diffusion of the large $[PtCl_6]^{2-}$ ions through the polymer matrix, while the absence of copper clusters may be due to its relatively low reduction potential.

## NORCOONa Method

In a modification of the strategy represented in Fig. 5, carboxylic acid groups are first converted to the sodium carboxylate form by soaking in aqueous NaOH; transition metal and rare earth ions are then substituted for $Na^+$ ions by immersion of the sodium carboxylate functionalized polymer in an aqueous metal salt solution.[51] This method, represented in Fig. 7, can be used to increase the rate and extent of metal uptake into diblock copolymer films. The Ag loading capacity of sodium carboxylate functionalized films was explored following several loading and reduction sequences. The relationship between the extent of $Ag^+$ loading and cluster size during a single sequence was also studied for the carboxylic acid functionalized films.

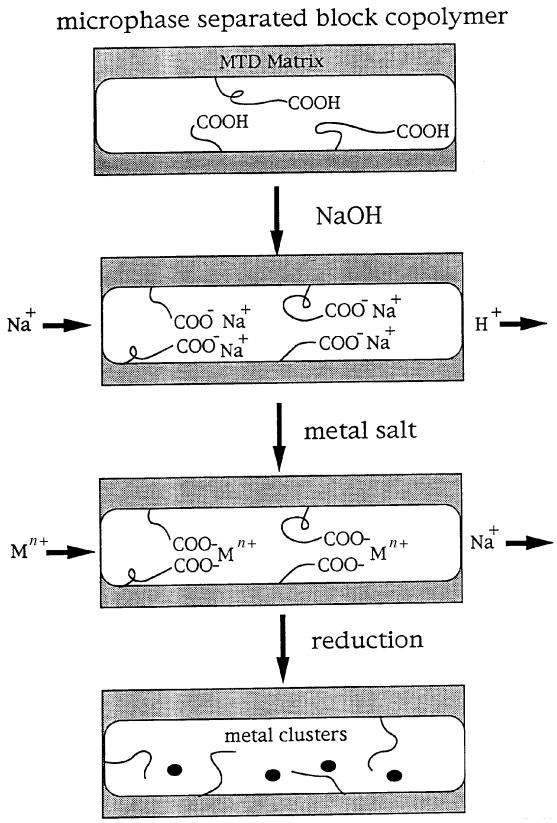


**Fig. 7** Modified scheme to facilitate metal ion loading into the block copolymer nanoreactors

Conversion of carboxylic acid groups within $[MTD]_{400}[NORCOOH]_{50}$ diblock copolymers to the sodium carboxylate form, $[MTD]_{400}[NORCOONa]_{50}$, resulted in large increases in both the rate and extent of transition metal and rare earth ion uptake from metal acetates, chlorides, nitrates and sulfates. For Co-, Au-, Pd- and Ni-containing compounds, significant loading could often be achieved from 0.005 M aqueous metal salt solutions into 10 μm thick $[MTD]_{400}[NORCOONa]_{50}$ films within hours, whereas no loading was observed into $[MTD]_{400}[NORCOOH]_{50}$ films. The improvement in loading is due largely to the acetate ion's much lower stability constant with $Na^+$ ($K_1 \approx 0.7$ l mol$^{-1}$), than with $H^+$ ($K_1 \approx 6.3 \times 10^4$ l mol$^{-1}$). This allows transition metal and rare earth ions ($K_1 \approx 3$–$1600$ l mol$^{-1}$) to displace the weakly bound $Na^+$ ions more easily than the much more strongly bound $H^+$ ions.

A 10 μm thick $[MTD]_{400}[NORCOONa]_{50}$ film was subjected to several loading and reduction sequences and displayed equilibrium $Ag^+$ uptake capacities of 0.77, 0.69, 0.67 and 0.45 moles $Ag^+$ per mole COONa during the first, second, third and fourth loadings, respectively. This corresponds to a cumulative loading of approximately 26 wt% Ag in the polymer–Ag composite. The decrease in equilibrium $Ag^+$ loading following several sequences is probably due to the increasing volume fraction of Ag nanoclusters within the polyNORCOONa domains, which may sterically prevent exchange between $Na^+$ and $Ag^+$ ions. Mean crystal sphere diameters of 37, 50, 64 and 65 Å were estimated from WAXS data following the first, second, third and fourth loading and reduction sequence, respectively. Thus, Ag nanoclusters produced in early loading and reduction cycles act as nucleation sites for further cluster growth. During a single sequence, the cluster size within diblock copolymer is relatively insensitive to the extent of $Ag^+$ uptake for loadings between 40 and 500 mg $Ag^+$ per g polyNORCOOH, consistent with a nucleation-controlled cluster formation process. It is not known whether the observed mean cluster size of *ca.* 30 Å is a result of thermodynamic or kinetic constraints.[51]

## Summary

A brief survey has been presented to summarize block-copolymer-based strategies for nanocluster/nanocomposite synthesis. One strategy involves synthesis of suitable organometallic monomers that can be incorporated into a block copolymerization scheme such as ring-opening metathesis polymerization. Thermodynamically driven microphase separation assembles the metal-containing repeat units into isolated domains in which the metal clusters are formed by appropriate reduction techniques. A second strategy involves copolymerization/microphase separation of a block copolymer in which one of the block sequences contains ion-sequestering ligands such as carboxylic acid groups. In this more general nanoreactor scheme a wide variety of metal ions can be selectively loaded into the copolymer morphology and subsequently reduced to form clusters. Although the present review has focused on zerovalent metal clusters, many other possibilities, such as the production of metal sulfides, selenides or oxides, are readily achieved.

A few properties and potential applications of the metal-cluster-containing nanocomposites have been mentioned here. Large dielectric anisotropy appears to require nearly percolating clusters in one of the domains and this has not been achieved in work to date. Hints of exceedingly large anisotropies in electrical conductivity have been demonstrated although the magnitudes of all the conductivities measured to

date are low. Perhaps surprisingly, palladium metal clusters embedded in the block copolymer matrix retain very active catalytic properties when examined in the context of olefin and butadiene hydrogenation reactions. Evidently, whatever the nature of the surface adsorption by the polymer chains, these species are readily displaced by the unsaturated small molecules as they participate in the metal-surface-catalyzed hydrogenation reactions. The intriguing possibility arises for using these nanocomposite films both as a catalyst and as a part of a product separation scheme in a suitably designed reactor.

Although not mentioned above, there are many more potential applications for metal-cluster-containing films, including those relying on magnetic and optical phenomena.[43,51] The fact that the well-dispersed metal clusters in these block-copolymer-based nanocomposites are smaller than the wavelength of visible light eliminates significant scattering of light. This fact, coupled with the strong absorbances offered by the surface plasmon phenomenon at specific wavelengths, makes it possible to imagine producing transparent metal-containing nanocomposite films in a wide range of colors and/or with light absorption selectivity in the UV or IR portion of the spectrum.

There are many unanswered questions surrounding the formation of the metal clusters in the block copolymer domains. The enormous viscosites of bulk polymer systems always leads to the likelihood that kinetically locked systems are being considered instead of thermodynamically equilibrated materials. Some aspects of the fundamental competition between nucleation and growth were addressed above. The degree to which metal-binding ligands on the copolymer repeat units retard cluster growth is not well understood. The competing possibilities for forming alloys, core-shell clusters and side-by-side populations of clusters also need to be explored in systematic detail in order to exploit fully the nanocluster synthesis schemes described here.

## References


1 N. L. Pocard, D. C. Alsmeyer, R. L. McCreery, T. X. Neenan and M. R. Callstrom, *J. Am. Chem. Soc.*, 1992, **114**, 769.
2 K. J. Klabunde, Y. X. Li and B. J. Tan, *Chem. Mater.*, 1991, **3**, 30.
3 S. C. Davis and K. J. Klabunde, *Chem. Rev.*, 1982, **82**, 153.
4 C. N. Satterfield, in *Heterogeneous Catalysis in Industrial Practice*, 2nd edn., McGraw-Hill, New York, 1991, p. 175.
5 T. Yonezawa and N. J. Toshima, *J. Mol. Catal.*, 1993, **83**, 167.
6 B. H. Sohn and R. E. Cohen, *Chem. Mater.*, 1997, **9**, 264.
7 Y. Ichiyanagi and Y. Kimishima, *Jpn. J. Appl. Phys.*, 1996, **35**, 2140.
8 D. L. Lesliepelecky and R. D. Rieke, *Chem. Mater.*, 1996, **8**, 1770.
9 M. Gao, Y. Yang, B. Yang and J. Shen, *J. Chem. Soc., Faraday Trans.*, 1995, **91**, 4121.
10 R. H. Magruder III, R. A. Weeks, S. H. Morgan, Z. Pan, D. O. Henderson and R. A. Zuhr, *J. Non-Crystal. Solids*, 1995, **193**, 546.
11 K. Puech, F. Henari, W. Blau, D. Duff and G. Schmid, *Europhys. Lett.*, 1995, **32**, 119.
12 D. W. Bahnemann, *Isr. J. Chem.*, 1993, **33**, 115.
13 J. Perrin, B. Despax and E. Kay, *Phys. Rev. B*, 1985, **32**, 719.
14 F. Hache, D. Richard and C. Flytzanis, *J. Opt. Soc. Am. B*, 1986, **3**, 1647.
15 G. D Stucky, *Naval Res. Rev.*, 1991, **3**, 28.
16 A. Henglein, *Chem. Rev.*, 1989, **89**, 1861.
17 G. D. Stucky and J. E. MacDougall, *Science*, 1990, **247**, 669.
18 W. P. Halperin, *Rev. Mod. Phys.*, 1986, **58**, 533.
19 G. C. Bond, *Surf. Sci.*, 1985, **156**, 966.
20 K. J. Klabunde, J. Habdas and G. Cadenas-Trivino, *Chem. Mater.*, 1989, **1**, 481.
21 M. S. El-Shall and W. Slack, *Macromolecules*, 1995, **28**, 8456.
22 J. H. Golden, H. Deng, F. J. DiSalvo, J. M. J. Frechet and P. M. Thompson, *Science*, 1995, **268**, 1463.
23 A. Heilmann and C. Hamann, *Prog. Colloid Polym. Sci.*, 1991, **85**, 102.
24 J. J. Watkins and T. J. McCarthy, *Chem. Mater.*, 1995, **7**, 1991.
25 M. Möller, *Synth. Met.*, 1991, **41–43**, 1159.
26 R. Saito, S. Okamura and K. Ishizu, *Polymer*, 1992, **33**, 1099.
27 J. P. Spatz, A. Roescher and M. Möller, *Polym. Prep.*, 1996, **37**, 409.
28 Y. Ng Cheong Chan, R. R. Schrock and R. E. Cohen, *Chem. Mater.*, 1992, **4**, 24; *J. Am. Chem. Soc.*, 1992, **114**, 7295.
29 M. Moffitt and A. Eisenberg, *Macromolecules*, 1997, **30**, 4363.
30 Y. Ng Cheong Chan, G. S. Craig, R. R. Schrock and R. E. Cohen, *Chem. Mater.*, 1992, **4**, 885.
31 B. H. Sohn and R. E. Cohen, *Chem. Mater.*, 1997, **9**, 264.
32 B. H. Sohn, G. C. Papaefthymiou and R. E. Cohen, *J. Magn. Magn. Mater.*, in press.
33 V. Sankaran, C. C. Cummins, R. R. Schrock, R. E. Cohen and R. J. Silbey, *J. Am. Chem. Soc.*, 1990, **112**, 6858.
34 V. Sankaran, R. E. Cohen, C. C. Cummins and R. R. Schrock, *Macromolecules*, 1991, **24**, 6664.
35 C. C. Cummins, M. D. Beachy, R. R. Schrock, M. G. Vale, V. Sankaran and R. E. Cohen, *Chem. Mater.*, 1991, **3**, 1153.
36 C. C. Cummins, R. R. Schrock and R. E. Cohen, *Chem. Mater.*, 1992, **4**, 27.
37 V. Sankaran, J. Yue, R. E. Cohen, R. R. Schrock and R. J. Silbey, *Chem. Mater.*, 1993, **5**, 1133.
38 J. Yue, V. Sankaran, R. E. Cohen and R. R. Schrock, *J. Am. Chem. Soc.*, 1993, **115**, 4409.
39 J. Yue and R. E. Cohen, *Supramol. Sci.*, 1995, **1**, 117.
40 R. S. Kane, R. J. Silbey and R. E. Cohen, *Chem. Mater.*, 1996, **8**, 1919.
41 R. T. Clay and R. E. Cohen, *Supramol. Sci.*, 1995, **2**, 183; *ibid.*, 1997, **4**, 113.
42 B. H. Sohn and R. E. Cohen, *Acta Polym.*, 1996, **47**, 340.
43 (*a*) B. H. Sohn and R. E. Cohen, *J. Appl. Polym. Sci.*, 1997, **65**, 723; (*b*) B. H. Sohn, Ph.D. Thesis, Massachusetts Institute of Technology, Cambridge, MA, USA, 1996.
44 K. Ishizu, Y. Yamada, R. Saito, T. Kanbara and T. Yamamoto, *Polymer*, 1993, **34**, 2257.
45 A. R. Blythe, in *Electrical Properties of Polymers*, Cambridge University Press, Cambridge, UK, 1979.
46 J. F. Ciebien, R. E. Cohen and A. Duran, *Supramol. Sci.*, submitted.
47 J. F. Ciebien, Ph.D. Thesis, Massachusetts Institute of Technology, Cambridge, MA, USA, 1997.
48 V. Ponec and G. C. Bond, in *Catalysis by Metals and Alloys*, Elsevier, Amsterdam, The Netherlands, 1995, pp. 227–279, 477, 482, 491, 500–504.
49 H. E. Swanson and E. Tatge, *U.S. National Bureau of Standards Standard X-Ray Diffraction Patterns*, NBS Circular 539, U.S. Government Printing Office, Washington DC, 1953, vol. 1.
50 H. P. Klug and L. E. Alexander, in *X-Ray Diffraction Procedures*, Wiley, New York, 1954, p. 491.
51 R. T. Clay, Ph.D. Thesis, Massachusetts Institute of Technology, Cambridge, MA, USA, 1997.



*Received in Montpellier, France, 14th October* 1997;
*Paper* 7/09233D